

Supporting Information

Polyoxometalate loaded reduced graphene oxide modified metal vanadate catalysts for photoredox reactions through Indirect Z-scheme mechanism

Soumita Samajdar^{#a,c}, Gajiram Murmu^{#b,c}, Maitrayee Biswas^a, Srikrishna Manna^{c,d}, Sumit Saha^{b,c*}, Srabanti Ghosh^{a,c*}

^aEnergy Materials & Devices Division, CSIR - Central Glass and Ceramic Research Institute, Kolkata, West Bengal 700032, India

^bMaterials Chemistry Department, CSIR - Institute of Minerals & Materials Technology, Bhubaneswar, Odisha 751013, India

^cAcademy of Scientific and Innovative Research (AcSIR), Ghaziabad, Uttar Pradesh 201002, India

^dSpecialty Glass Division, CSIR - Central Glass and Ceramic Research Institute, Kolkata, West Bengal 700032, India

Equal Contributions

*Corresponding authors

E-mail address: srabanti@cgcri.res.in (Srabanti Ghosh), sumitsaha@immt.res.in (Sumit Saha)

List of Figures:

Fig. S1. PXRD Pattern of RPOM, AV, RPOM-AV3, CV and RPOM-CV3.

Fig. S2. Raman spectra of RPOM, AV, CV, RPOM-AV3, and RPOM-CV3.

Fig. S3. FTIR spectra of pristine AV and CV.

Fig. S4. DRS of (a) AV, RPOM, RPOM-AV2 and RPOM-AV3, (b) CV, RPOM, RPOM-CV2 and RPOM-CV3.

Fig. S5. Tauc Plots of (a) AV, (b) CV, (c) RPOM, (d) RPOM-AV2, (e) RPOM-AV3, (f) RPOM-CV2, and (g) RPOM-CV3.

Fig. S6. TGA curve of (a) RPOM, RPOM-AV2, and RPOM-CV2, (b) Pristine AV and CV.

Fig. S7. Photoluminescence spectra of (a) AV, RPOM, RPOM-AV2, (b) CV, RPOM, RPOM-CV2 upon excitation at 375 nm.

Fig. S8. FESEM image of RPOM-AV3 and RPOM-CV3.

Fig. S9. (a) FESEM image of RPOM, and EDX elemental mapping of (b) C, (c) O, (d) P, (e) W.

Fig. S10. (a) TEM image of pristine AV at lower magnification and higher magnification (inset) (b) TEM image of pristine CV.

Fig. S11. TEM images of RPOM-AV3 and RPOM-CV3.

Fig. S12. N₂ adsorption and desorption isotherms of (a) RPOM-AV, (b) RPOM-CV, (c) RPOM. Inset of (a-c): Pore diameter distribution.

Fig. S13. Survey Spectra of (a) Pristine AV and RPOM-AV composites (b) Pristine CV and RPOM-CV composites.

Fig. S14. Core level XPS lineshape of (a) Ag 3d, (b) V 2p, (c) O 1s of pristine AV and RPOM-AV composites (d) C 1s lineshape (e) W 4f core level XPS lineshape of RPOM-AV composites.

Fig. S15. Core level XPS lineshape of (a) Cu 2p, (b) V 2p, (c) O 1s of pristine AV and RPOM-CV composites (d) C 1s lineshape (e) W 4f core level XPS lineshape of RPOM-CV composites.

Fig. S16. Linear Sweep Voltammograms of (a) AV, AV-POM, RPOM-AV, RGO-AV (b) CV, CV-POM, RPOM-CV, RGO-CV.

Fig. S17. Bode Plots of (a) AV, RPOM, RPOM-AV2 (b) CV, RPOM, RPOM-CV2.

Fig. S18. Width of space charge region of (a) RPOM, (b) AV, (c) RPOM-AV2, (d) CV, and (e) RPOM-CV2.

Fig. S19. UV-Vis spectra of RB adsorption in the presence of RPOM-AV2 and MB photocatalytic degradation in the presence of RPOM-CV2.

Fig. S20. Effect of different sacrificial agents on the MB dye degradation.

Fig. S21. (a) First-order kinetics plot of ($\ln C_0/C_t$) versus time (b) Photocatalytic Cr (VI) reduction using AV, RGO-AV, and RPOM-AV2 (c) Effect of different sacrificial agents on

the photocatalytic Cr (VI) reduction (d) Photocatalytic Cr(VI) reduction using RPOM-CV2 composites.

List of Tables:

Table S1. Current densities and charge transfer resistance of the RPOM-AV and RPOM-CV composites with different loading variations

Table S2. Rate constant values for the photoreduction of Cr (VI) using different photocatalysts

Table S3. Comparative study of polyoxometalate based composites towards photocatalytic MB degradation.

Table S4. Comparative study of various metal vanadate-based composites towards photocatalytic Cr (VI) reduction.

PXRD Spectra of RPOM-AV3 and RPOM-CV3

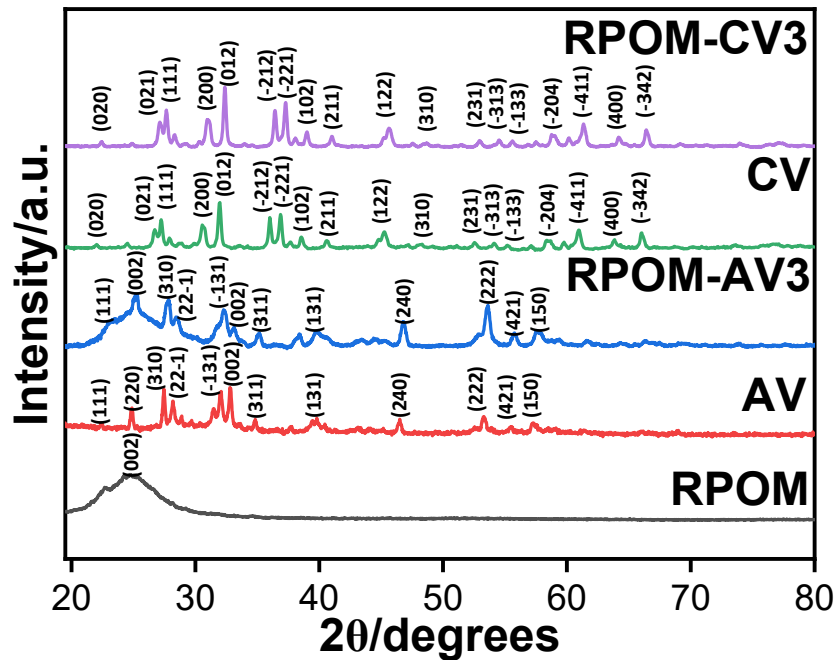


Fig. S1. PXRD Pattern of RPOM, AV, RPOM-AV3, CV and RPOM-CV3.

Raman spectra of RPOM, AV, CV RPOM-AV3 and RPOM-CV3

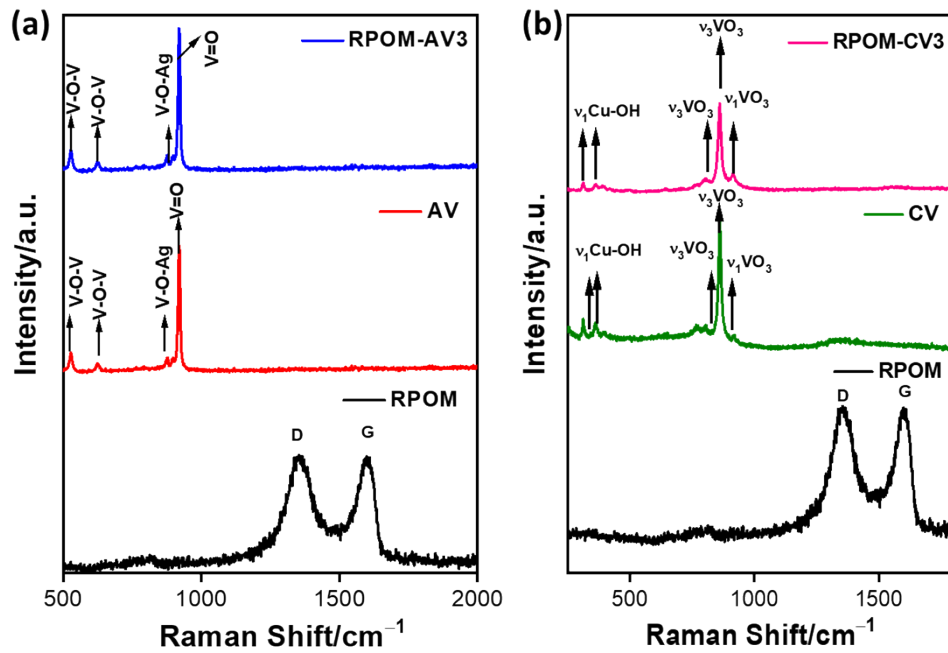


Fig. S2. Raman spectra of (a) RPOM, AV, RPOM-AV3, and (b) RPOM, CV, RPOM-CV3.

FTIR spectra of AV and CV

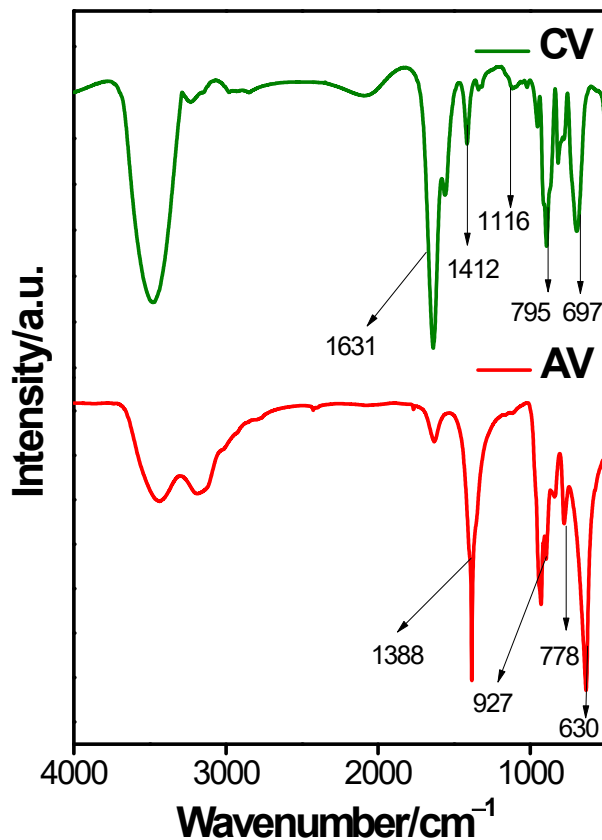


Fig. S3. FTIR spectra of pristine AV and CV.

UV-DRS spectra of AV, CV, RPOM, RPOM-AV and RPOM-CV

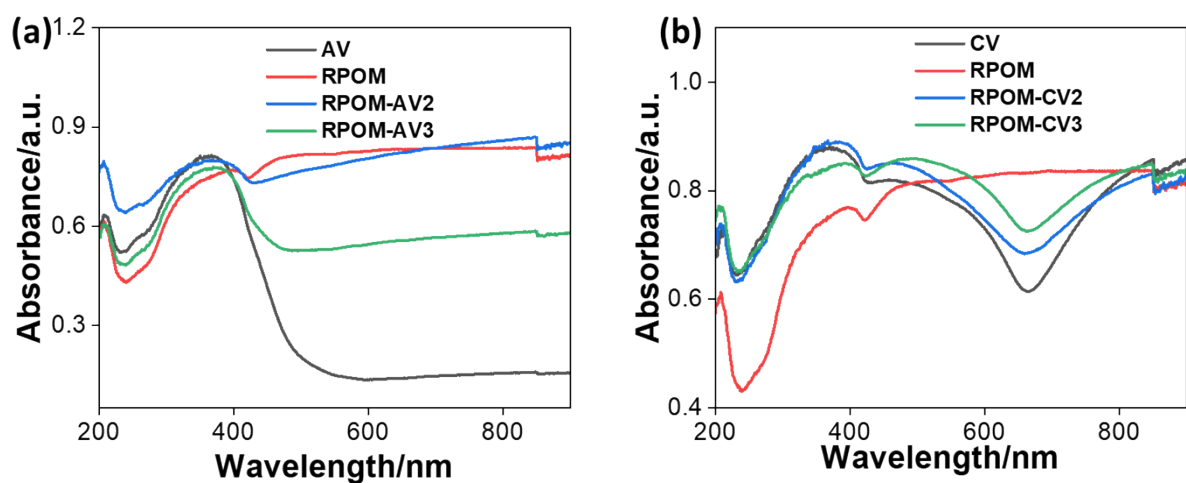


Fig. S4. DRS of (a) AV, RPOM, RPOM-AV2 and RPOM-AV3, (b) CV, RPOM, RPOM-CV2 and RPOM-CV3.

Tauc plot of AV, CV, RPOM, RPOM-AV and RPOM-CV

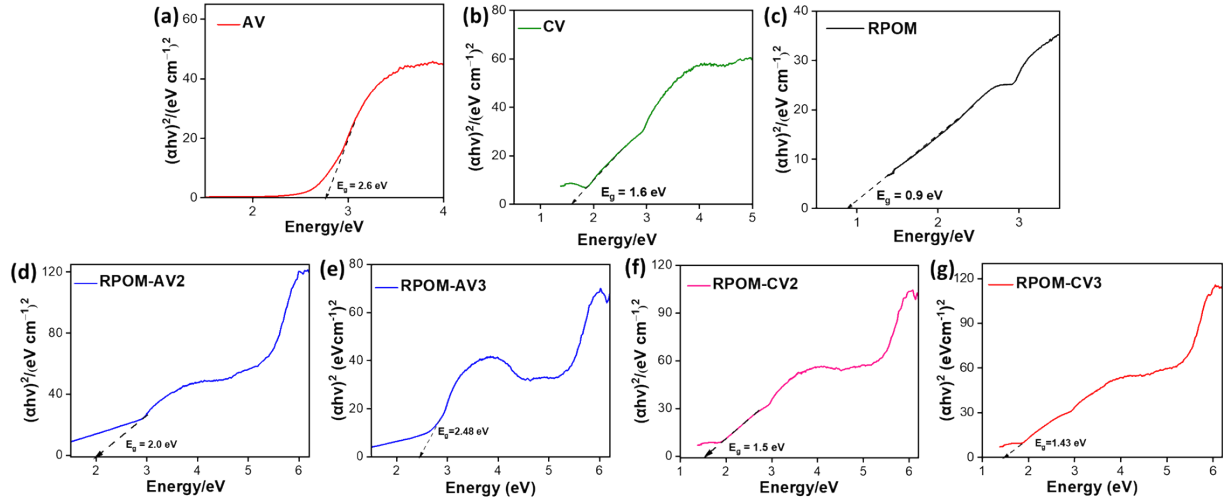


Fig. S5. Tauc Plots of (a) AV, (b) CV, (c) RPOM, (d) RPOM-AV2, (e) RPOM-AV3, (f) RPOM-CV2, and (g) RPOM-CV3.

TGA spectra of RPOM, AV, CV, RPOM-AV and RPOM-CV

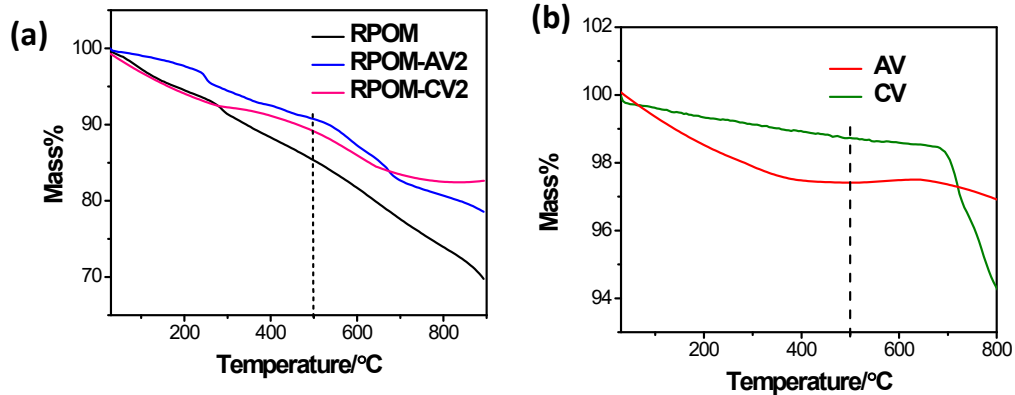


Fig. S6. TGA curve of (a) RPOM, RPOM-AV2, RPOM-CV2, and (b) Pristine AV and CV.

Photoluminescence (PL) spectra RPOM, AV, CV, RPOM-AV and RPOM-CV

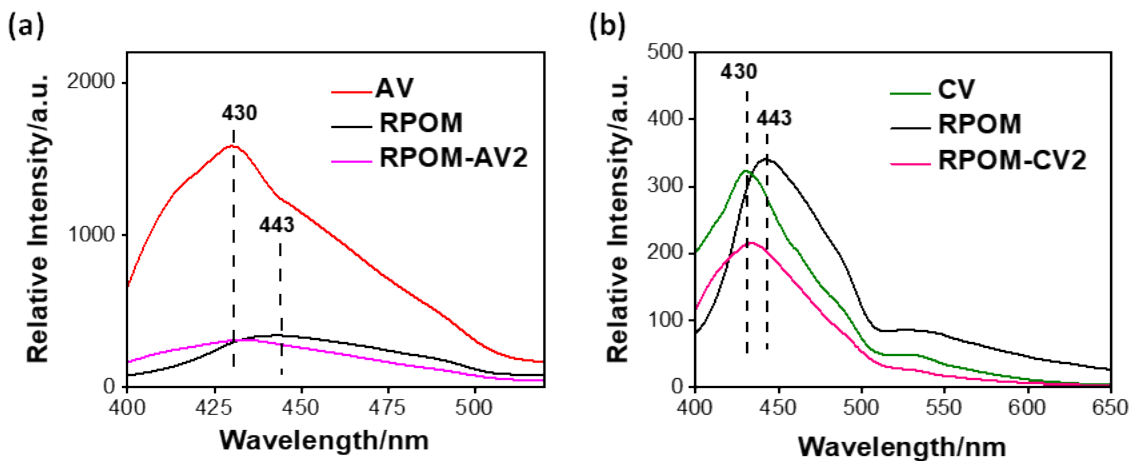


Fig. S7. Photoluminescence spectra of (a) AV, RPOM, RPOM-AV2, and (b) CV, RPOM, RPOM-CV2 upon excitation at 375 nm.

FESEM image of RPOM-AV3 and RPOM-CV3

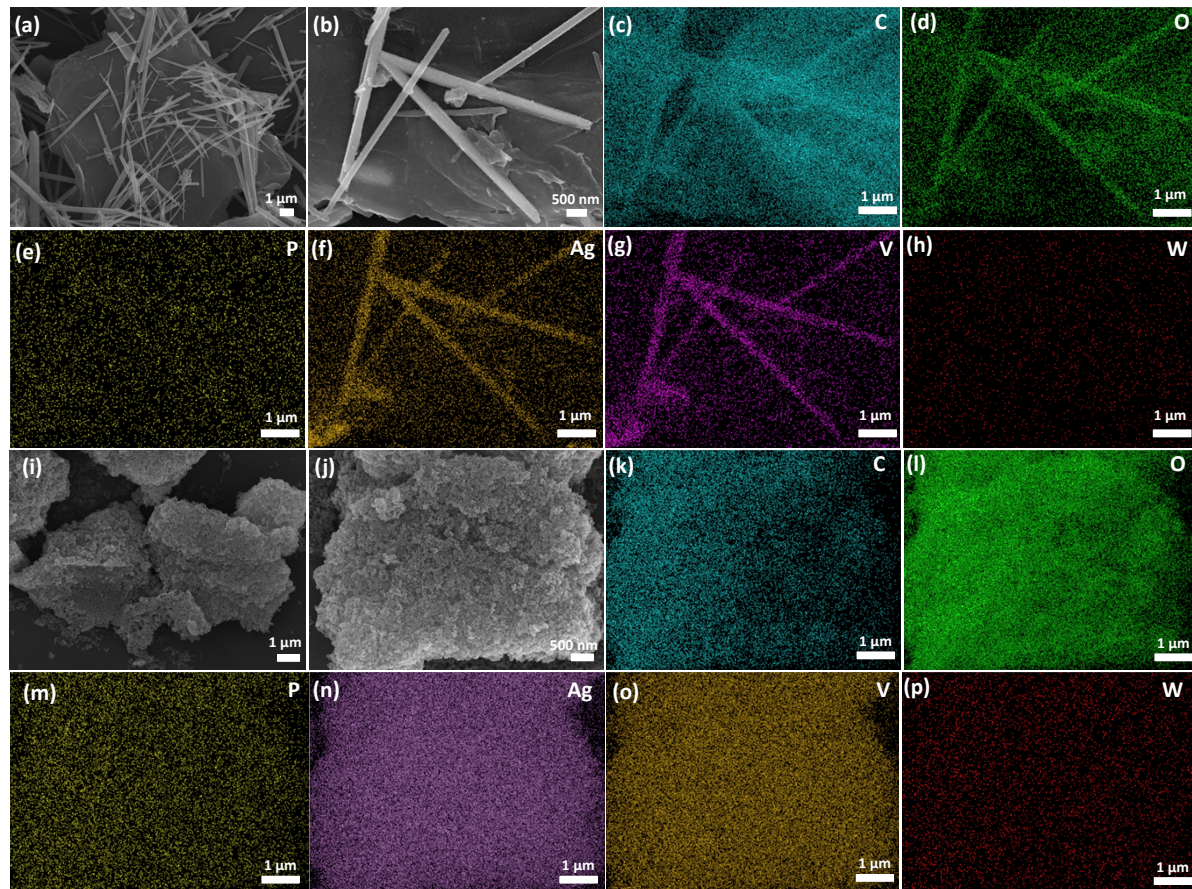


Fig. S8. FESEM images of RPOM-AV3 at (a) lower and (b) higher magnifications, EDX elemental mapping for (c) C, (d) O, (e) P, (f) Ag, (g) V, (h) W. FESEM images of RPOM-CV3 at (i) lower and (j) higher magnifications, EDX elemental mapping for (k) C, (l) O, (m) P, (n) Cu, (o) V, (p) W.

FESEM image of RPOM

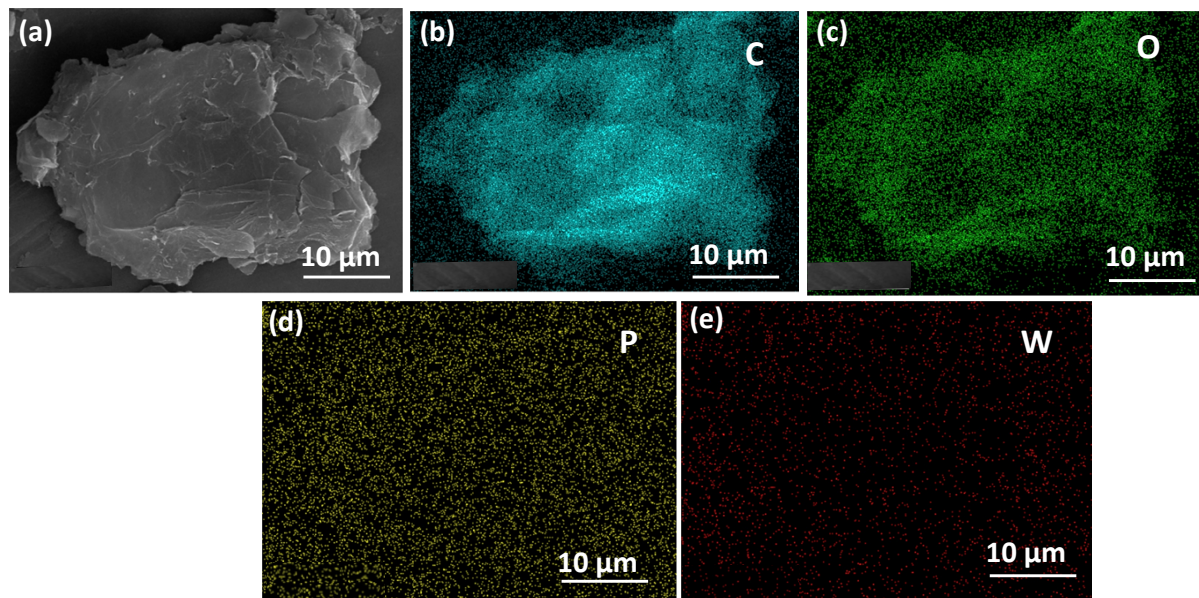


Fig. S9. (a) FESEM image of RPOM, and EDX elemental mapping of (b) C, (c) O, (d) P, (e) W.

TEM images of pristine AV and CV

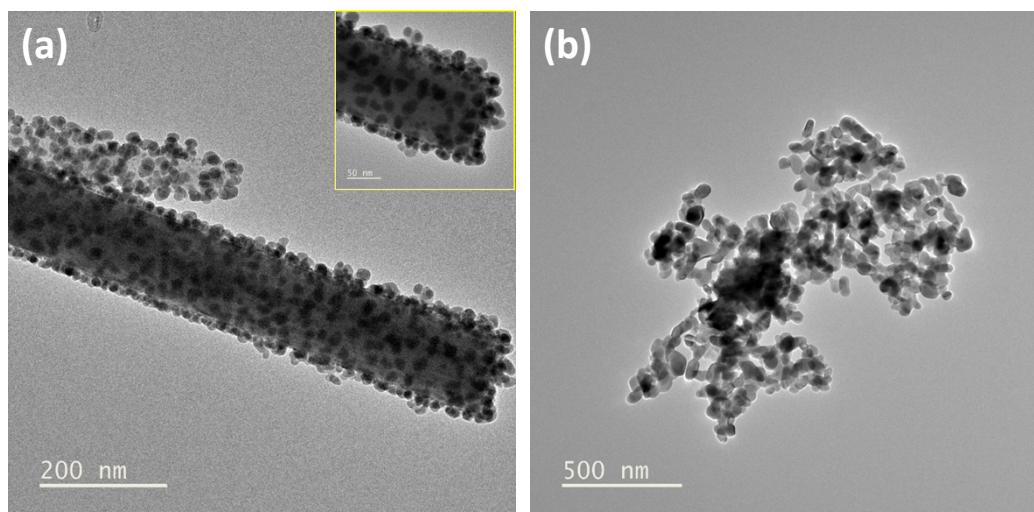


Fig. S10. (a) TEM image of pristine AV at lower magnification and higher magnification (inset), (b) TEM image of pristine CV.

TEM images of RPOM-AV3 and RPOM-CV3

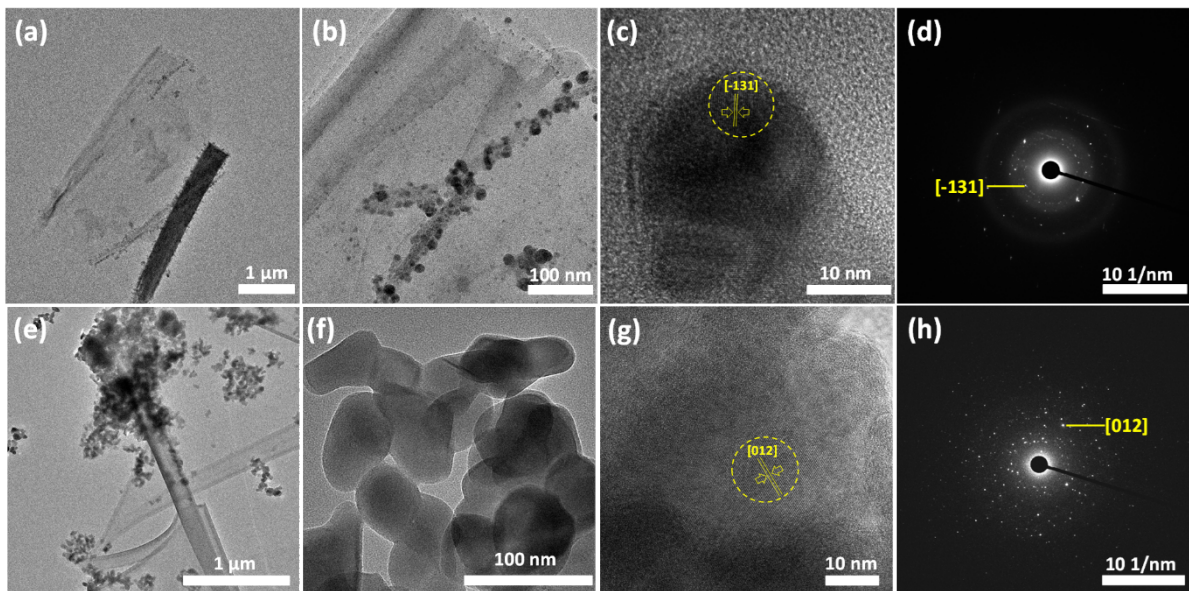


Fig. S11. TEM images of RPOM-AV3 at (a) lower and (b) higher magnifications, (c) HRTEM image, (d) SAED Pattern of RPOM-AV3. TEM images of RPOM-CV3 at (e) lower and (f) higher magnifications, (g) HRTEM image, (h) SAED Pattern of RPOM-CV3.

Surface area of RPOM, RPOM-AV, and RPOM-CV composites

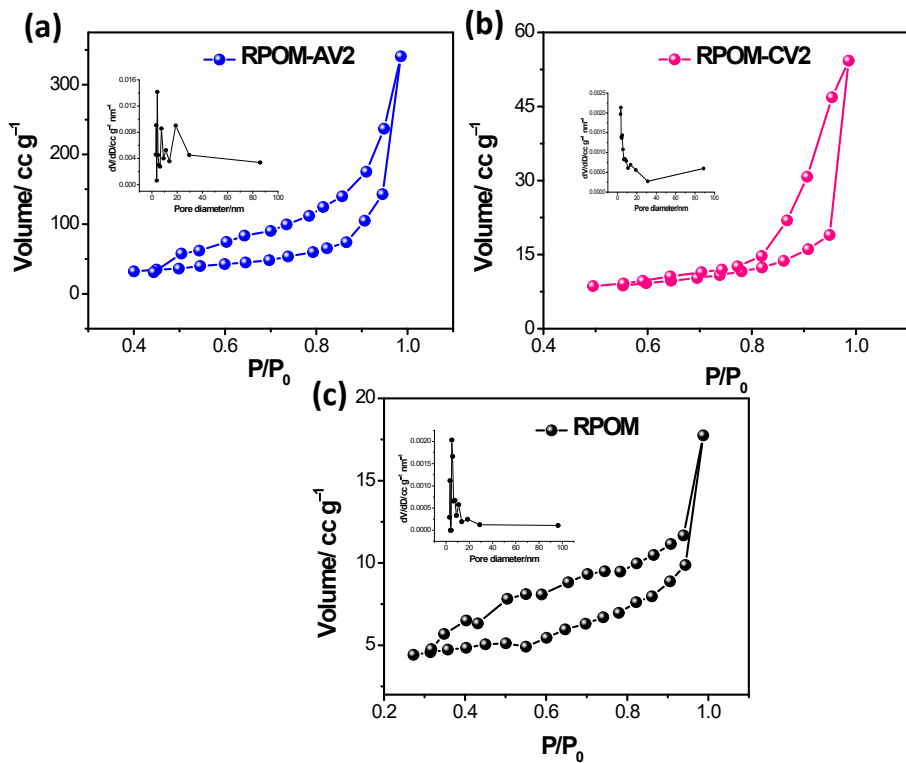


Fig. S12. N_2 adsorption and desorption isotherms of (a) RPOM-AV, (b) RPOM-CV, (c) RPOM. Inset of (a-c): Pore diameter distribution.

X-ray Photoelectron Spectroscopy of AV, RPOM-AV, CV, RPOM-CV composites

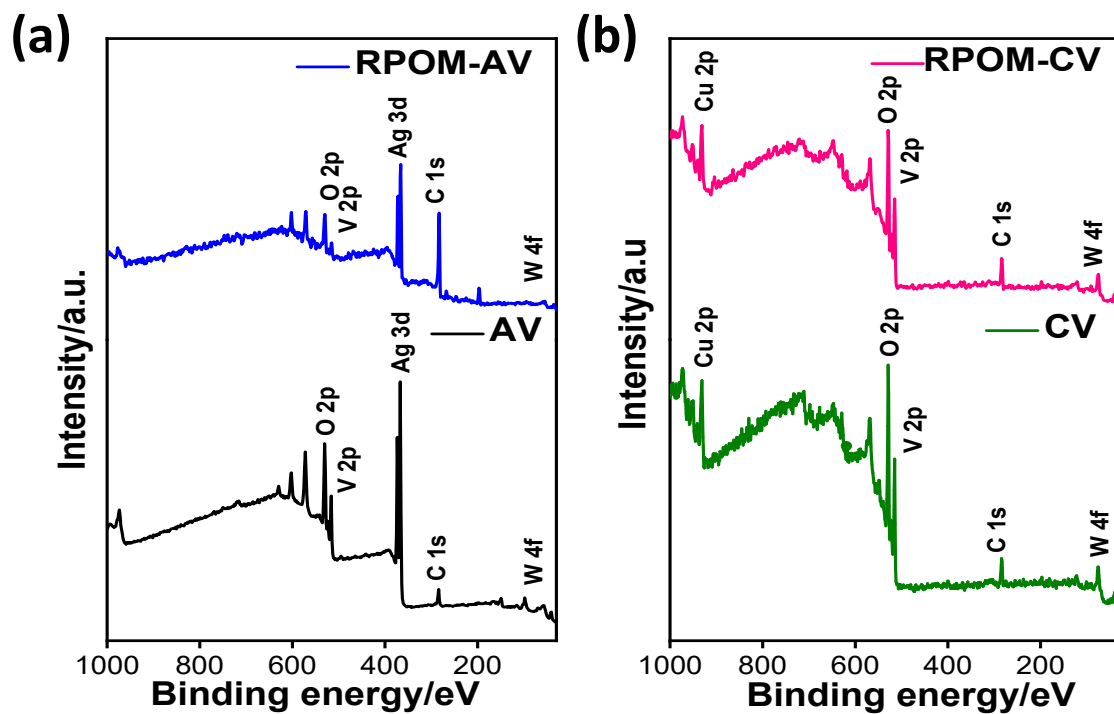


Fig. S13. Survey Spectra of (a) Pristine AV and RPOM-AV composites (b) Pristine CV and RPOM-CV composites.

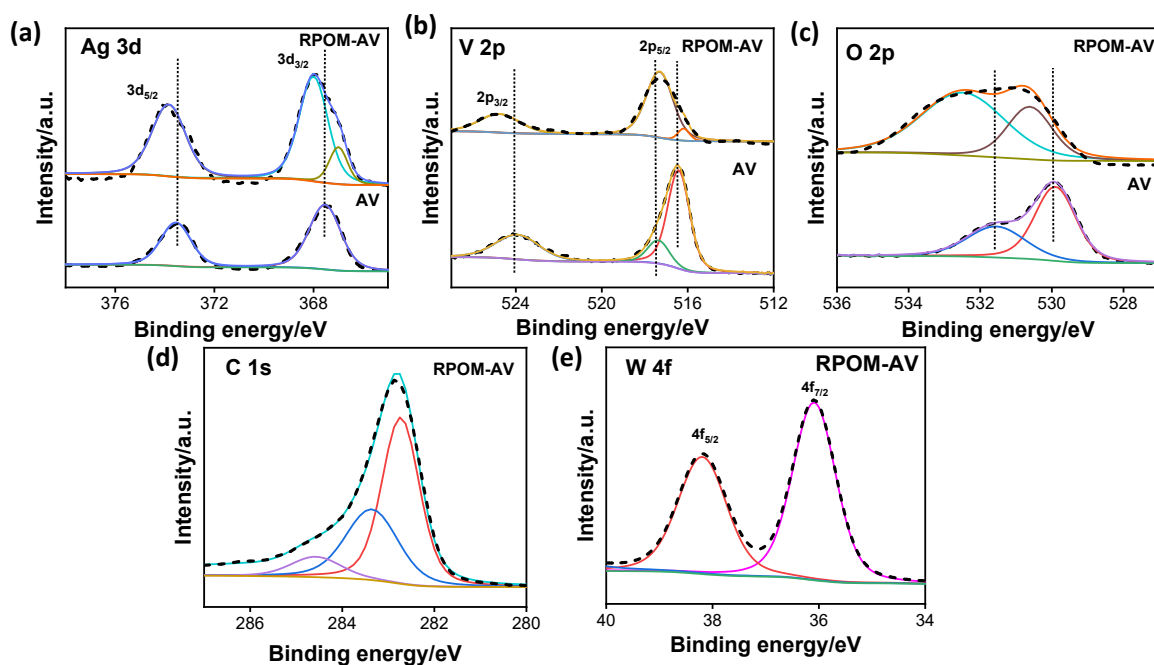


Fig. S14. Core level XPS lineshape of (a) Ag 3d, (b) V 2p, (c) O 1s of pristine AV and RPOM-AV composites (d) C 1s lineshape (e) W 4f core level XPS lineshape of RPOM-AV composites.

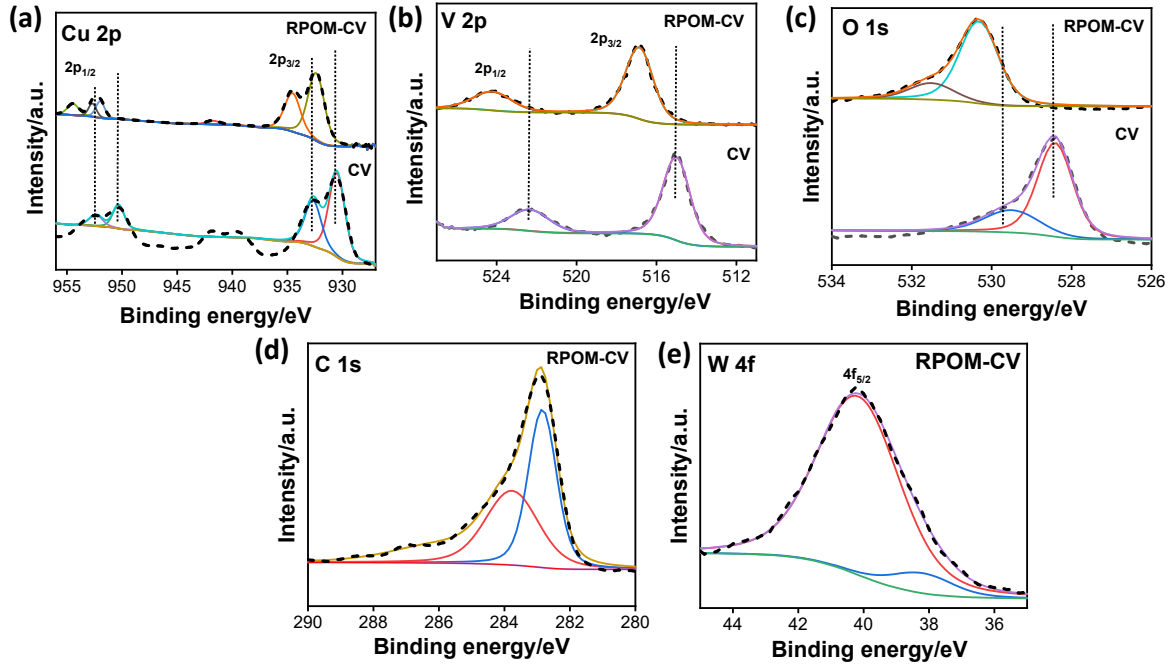


Fig. S15. Core level XPS lineshape of (a) Cu 2p, (b) V 2p, (c) O 1s of pristine AV and RPOM-CV composites (d) C 1s lineshape (e) W 4f core level XPS lineshape of RPOM-CV composites.

Linear Sweep Voltammograms (LSV) plot of AV, CV, AV-POM, CV-POM, RGO-AV, RGO-CV, RPOM-AV, RPOM-CV

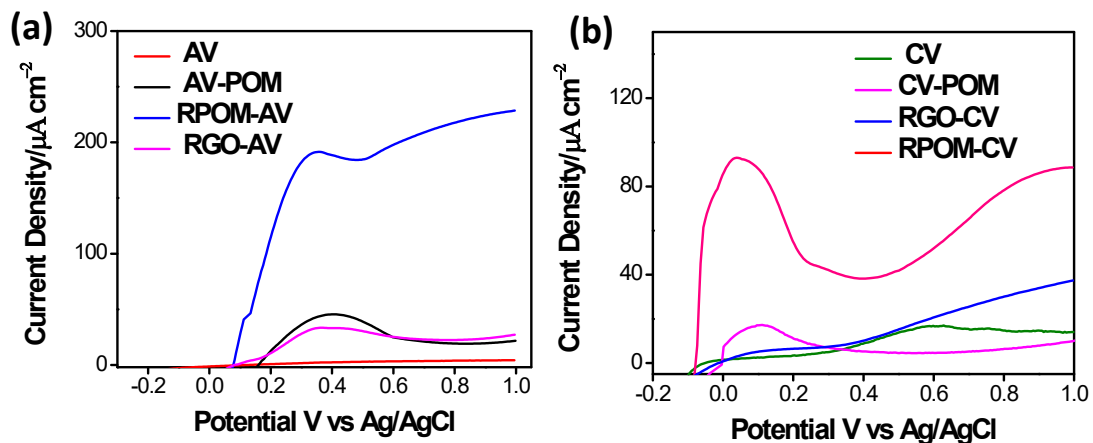


Fig. S16. Linear Sweep Voltammograms of (a) AV, AV-POM, RPOM-AV, RGO-AV and (b) CV, CV-POM, RPOM-CV, RGO-CV.

Bode plot of AV, CV, RPOM, RPOM-AV2, and RPOM-CV2

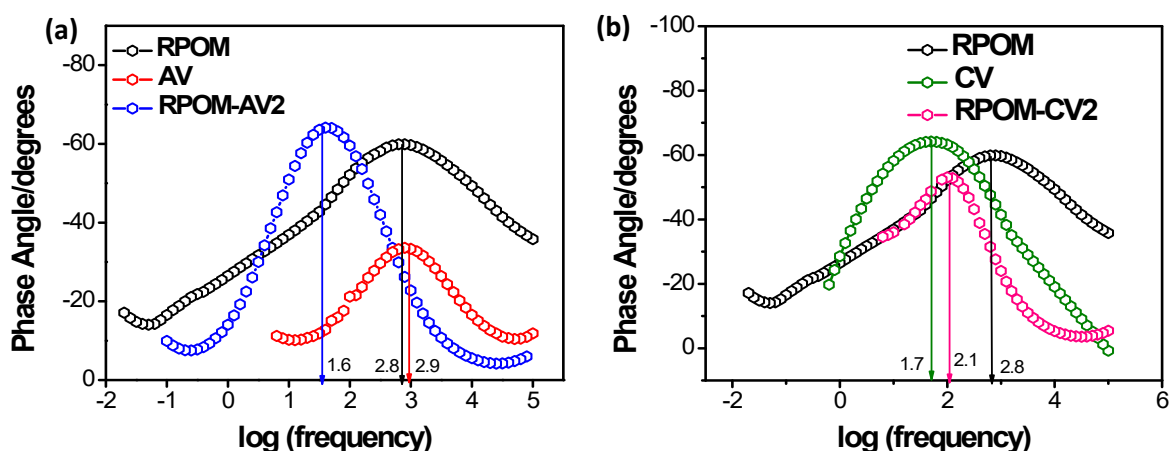


Fig. S17. Bode Plots of (a) AV, RPOM, RPOM-AV2 and (b) CV, RPOM, RPOM-CV2.

Width of space charge regions

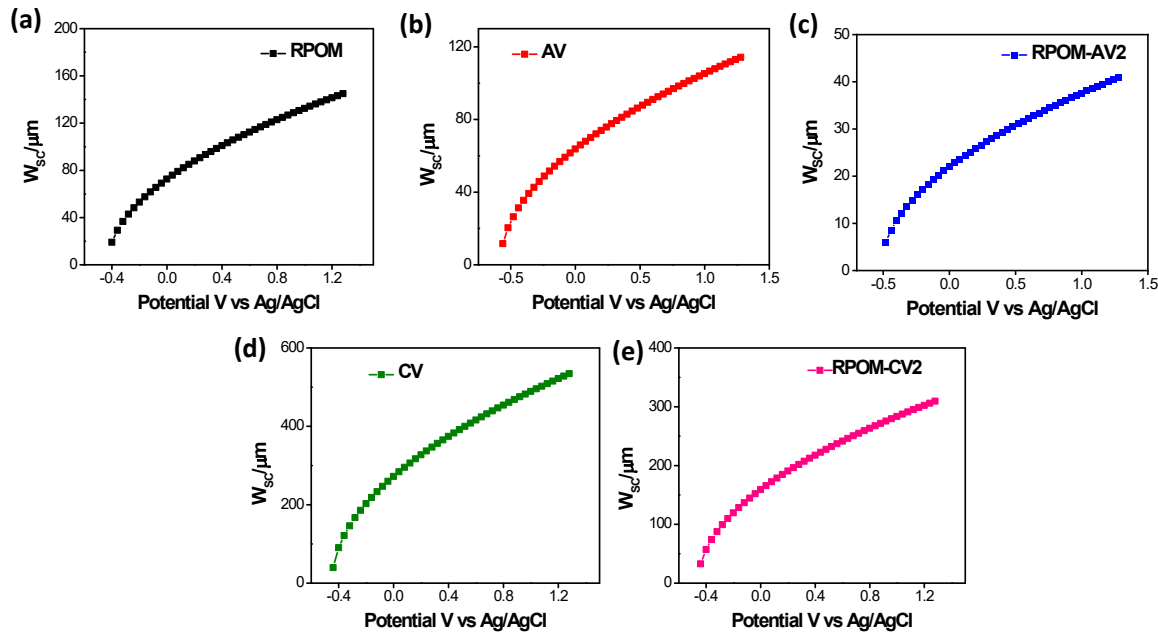


Fig. S18. Width of space charge region of (a) RPOM, (b) AV, (c) RPOM-AV2, (d) CV, and (e) RPOM-CV2.

UV-Vis spectra of RB adsorption in the presence of RPOM-AV2 and MB photocatalytic degradation in the presence of RPOM-CV2

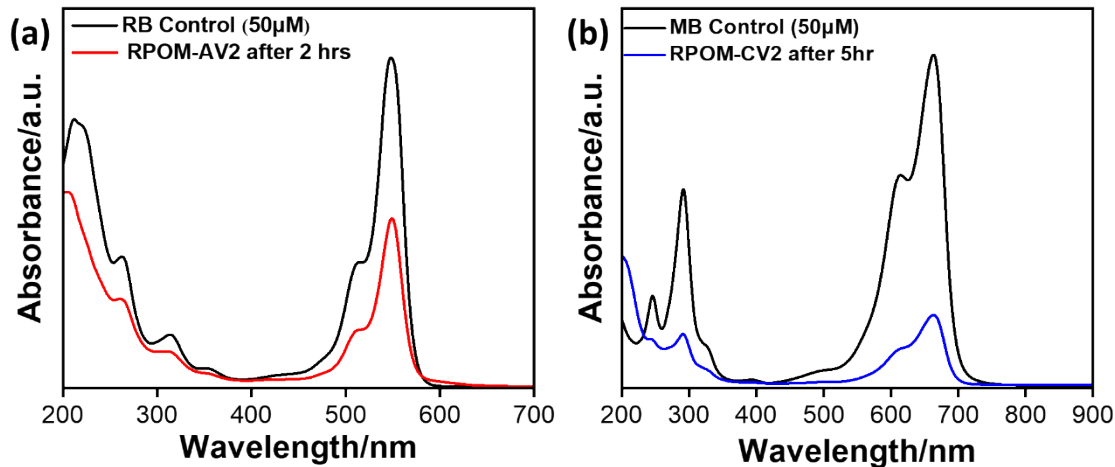


Fig. S19. (a) UV-visible absorption spectra for adsorption of RB dye in the presence of RPOM-AV2. (d) UV-visible absorption spectra for photocatalytic degradation of MB dye in the presence of RPOM-CV2.

Sacrificial agents experiment

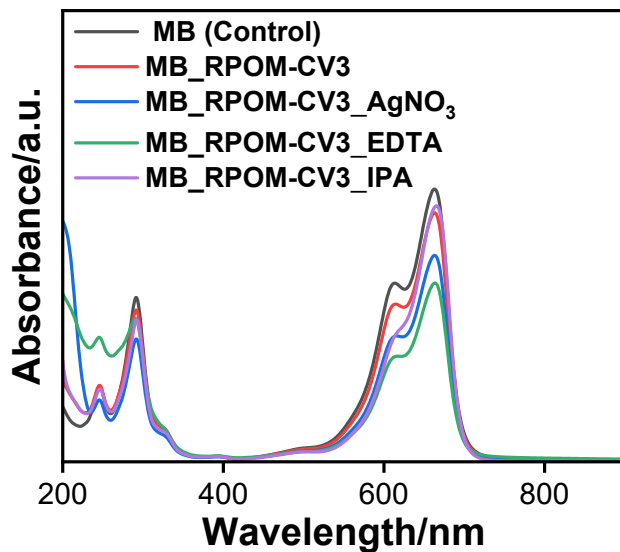


Fig. S20. Effect of different sacrificial agents on the MB dye degradation.

First-order kinetics plot

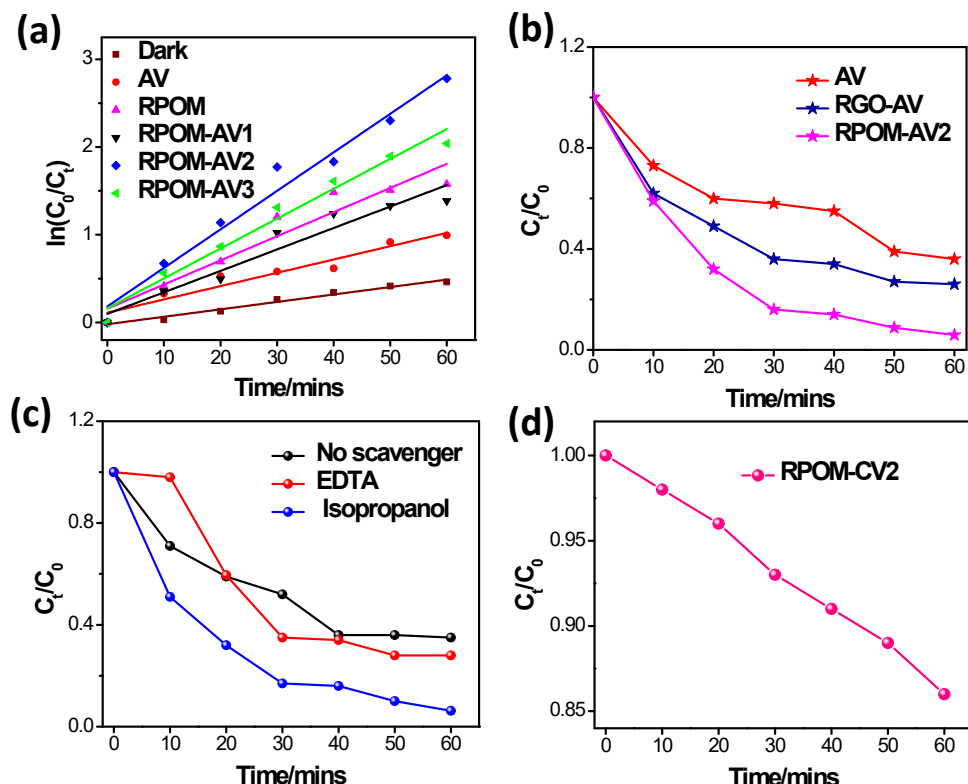


Fig. S21. (a) First-order kinetics plot of ($\ln C_0/C_t$) versus time, (b) Photocatalytic Cr (VI) reduction using AV, RGO-AV, and RPOM-AV2, (c) Effect of different sacrificial agents on

the photocatalytic Cr (VI) reduction, and (d) Photocatalytic Cr(VI) reduction using RPOM-CV2 composites.

Table S1. Current densities and charge transfer resistance of the RPOM-AV and RPOM-CV composites with different loading variations.

Material	Current Density at 0.9 V vs Ag/AgCl ($\mu\text{A cm}^{-2}$)	Charge Transfer Resistance (k Ω)
AV	4.4	11.3
RPOM	19.9	5.5
RPOM-AV1	60.1	0.65
RPOM-AV2	223.7	0.31
RPOM-AV3	46.5	4.2
<hr/>		
CV	14.6	18.9
RPOM-CV1	21.8	0.42
RPOM-CV2	85.8	0.38
RPOM-CV3	39.7	0.56

Table S2. Comparative study of the photocatalytic MB degradation using different POM-based photocatalysts.

Sl. No.	Catalysts	Catalyst Conc.	Light Source	MB Dye Conc.	Reaction Time	Degradation Efficiency	Reference
1.	(SiW ₁₂ O ₄₀) ⁴⁻	5 μM	Visible light (300 W Xe arc lamp)	50 μM	3 hrs	84 %	70
2.	NCW-NPs	50 mg	Visible light (300 W Xe lamp)	5 ppm	150 min	49.85%	71
3.	HPW@AG O-10	25 mg	Visible light (300	20 mg/L	150 min	84.02%	37

				W Xe lamp)			
4.	RPOM-CV3	1mg/ml	Visible light (112 W)	50 μ M	5 hrs	96%	Present Work

Table S3. Rate constant values for the photoreduction of Cr (VI) using different photocatalysts.

Sl. No.	Photocatalyst	Rate Constant (min^{-1})
1.	AV	0.008
2.	RPOM	0.028
3.	RPOM-AV1	0.024
4.	RPOM-AV2	0.044
5.	RPOM-AV3	0.034

Table S4. Comparative study of various metal vanadate-based composites towards photocatalytic Cr (VI) reduction.

Sl. No.	Material	Reduction Efficiency (%) of Cr (VI)	Time (mins)	Reaction Conditions	References
1.	Ag/AgBr /BiVO ₄	91.72%	60	Initial concentration: 10 ppm Light source: 300 W Xe lamp ($\lambda > 420 \text{ nm}$)	72
2.	BiVO ₄ /FeVO ₄ @rGO	90.9%	60	Initial concentration: 20 ppm Light source: 1 kW xenon lamp ($\lambda > 420 \text{ nm}$)	73
3.	BiVO ₄ / MXene	83.6%	120	Initial concentration: 10 ppm Illumination source: Visible light	74
4.	SnIn ₄ S ₈ / SmVO ₄	90.93 %	50	Initial concentration: 60 ppm Light source: 300 W halogen lamp ($\lambda > 420 \text{ nm}$)	75

5.	BiVO ₄ on B-Doped g-C ₃ N ₄	87%	30	Initial concentration: 20 ppm Light source: 150 W xenon lamp ($\lambda > 420$ nm)	76
6.	La,Gd- BiVO ₄	47%	100	Initial concentration: 20 ppm Light source: 400 W metal halide lamp	77
7.	RPOM- AV2	94 %	60	Initial concentration: 100 ppm Light source: 300 W Xe lamp	Present Work